GCOO#2090246, VOL 0, ISS 0

Architecture of a dinuclear Co(II) complex based on 3-amino-1,2,4-triazole-5-carboxylic acid: molecular structure, thermal behavior, optical properties, and DFT calculations

Sabr Ihassen, Youssef Arfaoui, Koen Robeyns, Timothy Steenhaut, Yaroslav Filinchuk, Axel Klein, and Hammouda Chebbi

QUERY SHEET

This page lists questions we have about your paper. The numbers displayed at left are hyperlinked to the location of the query in your paper.

The title and author names are listed on this sheet as they will be published, both on your paper and on the Table of Contents. Please review and ensure the information is correct and advise us if any changes need to be made. In addition, please review your paper as a whole for typographical and essential corrections.

Your PDF proof has been enabled so that you can comment on the proof directly using Adobe Acrobat. For further information on marking corrections using Acrobat, please visit http://journalauthors.tandf.co.uk/production/acrobat.asp; https://authorservices.taylorandfrancis.com/how-to-correct-proofs-with-adobe/

The CrossRef database (www.crossref.org/) has been used to validate the references.

AUTHOR QUERIES

Q1 Please check grant information for accuracy.

Q2 Please provide volume number and page number for Ref. 57.

Q3 Please provide location of the publisher for Ref. 74.

Q4 Please note that the ORCID section has been created from information supplied with your manuscript submission/CATS. Please correct if this is inaccurate.

PROOF ONLY

JOURNAL OF COORDINATION CHEMISTRY
https://doi.org/10.1080/00958972.2022.2090246

Taylor & Francis
Taylor & Francis Group

Check for updates

Architecture of a dinuclear Co(II) complex based on 3-amino-1,2,4-triazole-5-carboxylic acid: molecular structure, thermal behavior, optical properties, and DFT calculations

Sabr Ihassen[a], Youssef Arfaoui[a], Koen Robeyns[b], Timothy Steenhaut[b], Yaroslav Filinchuk[b], Axel Klein[c] and Hammouda Chebbi[d,e]

[a]Faculty of Sciences of Tunis, Laboratory of Characterizations, Applications and Modeling of Materials, University of Tunis El Manar, Tunis, Tunisia; [b]Institute of Condensed Matter and Nanosciences, Université catholique de Louvain, Louvain-la-Neuve 1348, Belgium; [c]Faculty of Mathematics and Natural Sciences, Department of Chemistry, Institute for Inorganic Chemistry, University of Cologne, Cologne 50939, Germany; [d]Preparatory Institute for Engineering Studies of Tunis, University of Tunis, Montfleury, Tunis 1089, Tunisia; [e]Faculty of Sciences of Tunis, Laboratory of Materials, Crystal Chemistry and Applied Thermodynamics, University of Tunis El Manar, Tunis, Tunisia

ABSTRACT

The dinuclear compound $[Co_2(Hatzc)_2(H_2O)_6](NO_3)_2{\cdot}4H_2O$ containing the polytopic ligand $Hatzc^- = 3$-amino-4*H*-1,2,4-triazole-5-carboxylate was synthesized and characterized. Single-crystal X-ray diffraction showed that two monoanionic *N,O*-chelating $Hatzc^-$ ligands bridge two Co(II) ions in a μ-*N*1,*N*2 fashion. Both Co(II) centers are further coordinated by three H_2O ligands making up an octahedral coordination. A complex network of intra- and intermolecular O–H···O and N–H···O hydrogen bonding interactions characterize the structure. Hirshfeld surface analysis, ATR–FTIR, and FT-Raman spectroscopy in combination with density functional theory (DFT) calculation of vibrational modes confirm this multitude of H bonds. Thermogravimetric and differential thermal analysis experiments under an argon atmosphere in the temperature range of 25–900 °C showed thermal stability till about 100 °C and multi-step decomposition yielding Co_2O_3 at about 280 °C. The octahedral environment of Co(II) was confirmed by UV–vis absorption spectroscopy, which shows weak absorption bands at around 520 nm assignable to electronic d–d transitions alongside with π–π* transitions dominating the 250–350 nm range. Time-dependent DFT calculated excited states agree very well in terms of energy match with the observed transitions. The direct and indirect optical band gap values were determined using the Tauc plot method to 3.33 eV and 2.75 eV, respectively, indicating semiconducting properties.

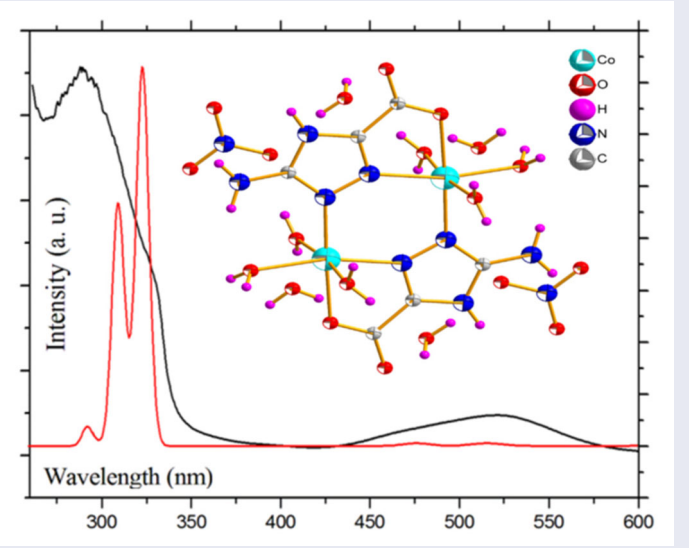
ARTICLE HISTORY
Received 24 February 2022
Accepted 3 June 2022

KEYWORDS
Dinuclear cobalt complex; polytopic ligand; 1,2,4-triazole-carboxylate; crystal structure; Hirshfeld surface analysis; UV–vis absorption; optical band gap; DFT calculations

CONTACT Hammouda Chebbi chebhamouda@Yahoo.fr University of Tunis, Preparatory Institute for Engineering Studies of Tunis, Jawaharlal NehruStreet, 1089 Montfleury, Tunis, Tunisia and Axel Klein axel.klein@uni-koeln.de University of Tunis, Preparatory Institute for Engineering Studies of Tunis, Jawaharlal NehruStreet, 1089 Montfleury, Tunis, Tunisia.

Supplemental data for this article is available online at https://doi.org/10.1080/00958972.2022.2090246.

© 2022 Informa UK Limited, trading as Taylor & Francis Group

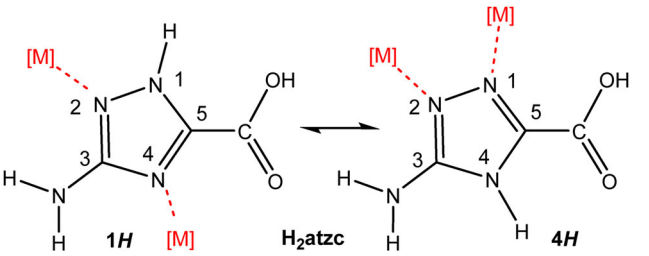


1. Introduction

In the quest for new materials with interesting electronic, optical, magnetic, or catalytic properties, coordination chemistry plays an important role. Combinations of metal ions and ligands can lead to various materials that are essentially held together by coordinative bonds and can be divided into 1-D, 2-D, or 3-D coordination polymers [1–14], including porous 3-D metal-organic frameworks (MOFs) [1, 2, 4–8], cyclic oligomers or clusters [8–17], and complexes or complex salts, frequently also called "0-D" materials [18–22]. Open shell transition metals with a preference for specific coordination symmetry can play a pivotal role in designing the structure of such materials, in contrast to full shell metal ions (full shell d block, s and p block). On the other hand, ions such as Ni(II) or Co(II) do not have a single preferred coordination sphere, they both can adopt the octahedral coordination but also tetrahedral, and even square planar for Ni. In recent years, the use of ditopic ligands that are multi-functional ligands with both bridging and chelating functionalities has allowed to further control the formation of coordination polymers and oligomers [4, 6, 8, 11–17, 23, 24]. Most of these ligands use O- or N-donor groups and show some degree of rigidity such as the N-containing pyrazoles, imidazoles, tetrazoles, triazoles, or polypyridines [23–29]. Carboxylate functions exhibit versatile coordination modes [30–32] and frequently a combination of rigid N-heterocyclic moieties with carboxylates is used for the design of polytopic ligands for coordination polymers [31, 32]. In recent years, 1,2,4-triazole and its derivatives gained interest as ligands to bridge metal ions with interesting structural, optical, catalytic, and magnetic properties [33–42].

Herein, 3-amino-1,2,4-triazole-5-carboxylic acid (H_2atzc, Scheme 1), comprising of a triazole ring with three N-donor atoms, an amino group, and a carboxylic acid group,

COLOR Online / B&W in Print



Scheme 1. Two tautomers of 3-amino-1,2,4-triazole-5-carboxylic acid (H_2atzc), left: 1*H* tautomer, right: 4*H* tautomer, allowing for two different μ-bridging motives upon metal coordination [M].

was chosen as the organic building unit since it has previously shown versatile coordination modes upon binding to metals in MOFs, coordination polymers, isolated complexes, and complex salts [25, 33–46]. The carboxylate group can act in a terminal or bridging coordination mode, and can also be used as a monodentate or bidentate coordination group. Furthermore, the two tautomers (Scheme 1) of H_2atzc can provide different bridging modes for dinuclear complexes. The slightly more stable 1H tautomer allows a μ-*N*2,*N*4 bridging, while the 4H tautomer enables a μ-*N*1,*N*2 bridge of two metal centers.

The crystal structure of the hemi-hydrate H_2atzc·0.5H_2O shows *N*1 and *N*4 protonated and an anionic carboxylate stabilized through intermolecular H bonding with the *N*4-H and the NH_2 functions [44] and both *N*1-H and *N*2-H tautomers have been observed in Ca, Sr, and Ba salts of $Hatzc^-$ [42]. The present study reports the synthesis of a new dinuclear Co(II) complex containing the 3-amino-4*H*-1,2,4-triazole-5-carboxylate ($Hatzc^-$) as μ-*N*1,*N*2-bridging ligand, the structural characterization by single crystal X-ray diffraction including Hirshfeld surface analysis, IR and Raman spectroscopic studies, thermal analysis [thermogravimetric (TGA)/differential thermal analysis (DTA)], and a detailed study of the optical properties. Density functional theory (DFT) calculations were used to assign vibrational bands. Time-dependent density functional theory (TD-DFT) calculations allowed to assign the observed UV–vis absorption bands.

2. Experimental

2.1. Materials and instrumentation

$Co(NO_3)_2$·6H_2O, 3-amino-1*H*-1,2,4-triazole-5-carboxylic acid and triethylamine (Et_3N) were obtained from Aldrich and used as received. The ATR-IR spectrum was recorded on a Bruker Alpha spectrometer equipped with a platinum ATR module (diamond crystal) from 400 to 4000 cm^{-1}. The Raman spectrum was recorded from 0 to 4000 cm^{-1} using a Bruker FT Raman RFS 100/S spectrometer equipped with a 1064 nm laser. The UV–vis absorption spectrum was recorded on a Shimadzu UV-1700 Pharma Spec spectrometer from 200 to 800 nm in absolute EtOH solution. The TGA and DTA measurements were carried out using a Netzsch STA 449 F3 Jupiter TGA/DTA device equipped with a stainless-steel oven housed in an argon-filled glovebox; 8.65 mg of compound was used for the measurement. The analysis was performed under an argon flow of 100 mL/min at a heating rate of 10 °C/min from 25 to 900 °C.

Table 1. Crystallographic data for $[Co_2(Hatzc)_2(H_2O)_6](NO_3)_2{\cdot}4H_2O$.

Chemical formula	$C_6H_{26}Co_2N_{10}O_{20}$
Formula weight (g mol^{-1})	676.23
Temperature (K)/Crystal size (mm^3)	100(2)/0.08 × 0.11 × 0.14
Crystal system/Space group	Monoclinic/$P2_1/n$ (No. 14)
Cell	
a (Å)	9.4642(3)
b (Å)	10.8650(7)
c (Å)	11.5451(4)
β (°)	104.843(4)
V (Å^3)/Z	1147.55(9) / 2
Density calculated (mg m^{-3})	1.957
Absorption coefficient (mm^{-1})	2.128
F(000)	692
θ range (°) for data collection	2.79–31.21
Index range	$-12 \le h \le 12$, $-12 \le k \le 12$, $-14 \le l \le 14$
Reflections collected	11681
Independent reflections/R_{int}	2371/0.028
Data/restraints/parameters	2371/0/190
Goodness-of-fit on F^2	1.033
Final R indices [$I > 2\sigma(I)$]	R_1: 0.0427, wR_2: 0.1131
R indices (all data)	R_1: 0.0432, wR_2: 0.1139
CCDC	2153469

2.2. Synthesis of the complex

An aqueous solution (20 mL of hot water) of 3-amino-1*H*-1,2,4-triazole-5-carboxylic acid (H_2atzc) (102 mg, 0.8 mmol) was added to an aqueous solution (25 mL) of $Co(NO_3)_2{\cdot}6H_2O$ (244 mg, 0.84 mmol) with constant stirring. The pH value of the resulting mixture was adjusted to 6 using Et_3N [39, 45]. The reaction mixture was heated at 70 °C, stirred for 2 h and subsequently left standing at room temperature. Over 1–2 weeks the solution evaporated almost to dryness and pink red block-shaped crystals were collected in several batches from brownish slurry. Some of them were suitable for single-crystal X-ray diffraction. Yield: 108 mg (0.16 mmol, 80%). Elemental analysis, found (Calcd.) for $C_6H_{26}Co_2N_{10}O_{20}$ (676.19 g/mol): C 10.63 (10.66), H 3.90 (3.88), N 20.69 (20.71) %.

2.3. X-Ray crystallography

Single-crystal X-ray diffraction data were measured at 100 K at the Swiss-Norwegian Beamlines (SNBL) at the European Synchrotron Radiation Facility (ESRF), Grenoble, France at a wavelength of 0.798 Å. The structure was solved by dual space direct methods using SHELXT [47] and refined by full-matrix least squares techniques on F^2 with SHELXL-2014/7 [48]. Hydrogen atoms of the water and NH_2 groups were idealized after being located in the density maps and refined as rigid groups able to rotate around the parent atom. The remaining H atoms were positioned geometrically and refined in riding.

2.4. DFT Calculations

The structure of the title compound was optimized using the DFT method and the Gaussian 09 program [49]. The calculations were performed using the hybrid B3LYP

COLOR Online / B&W in Print

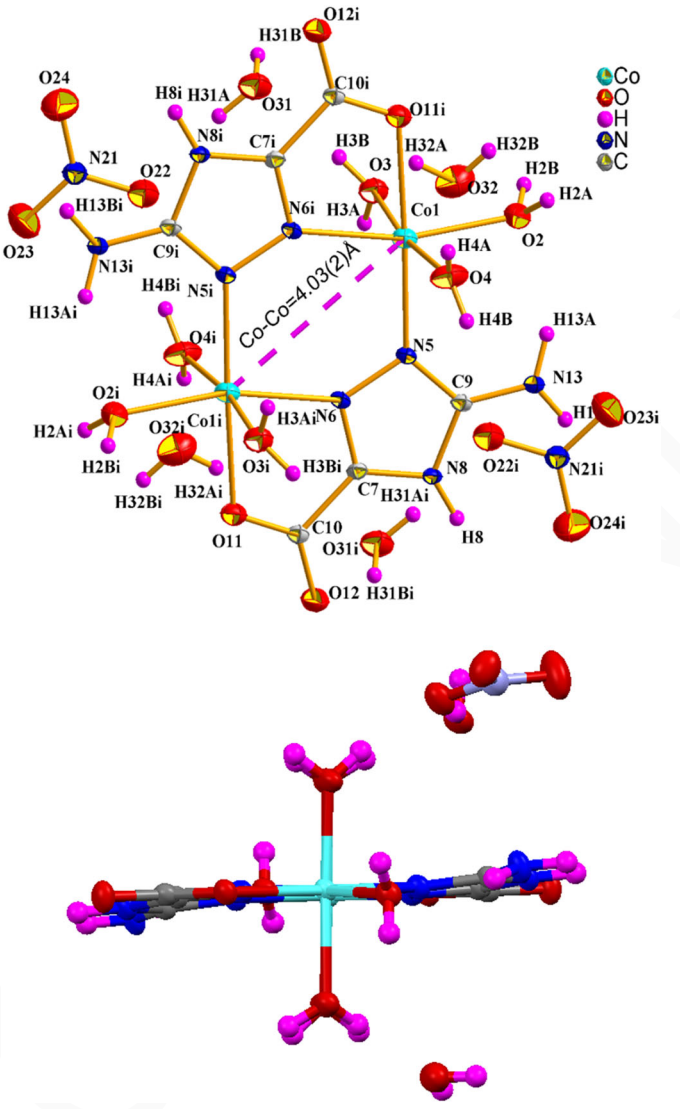


Figure 1. Two views of the unit cell contents of $[Co_2(Hatzc)_2(H_2O)_6](NO_3)_2{\cdot}4H_2O$ (thermal ellipsoids shown at the 50% probability level) [symmetry code: (i) $1-x, 1-y, 1-z$].

functional and the standard 6-311 + G(2d,2p) basis set for H, C, N, O [50–52], and LANL2DZ for Co [38]. Input geometric structure of these compounds is based on the optimum configurations that have been obtained from the single-crystal structure. The DFT calculations were carried out unrestricted (uB3LYP), with a charge = 0 and both Co^{2+} having a high-spin $t_{2g}{}^5e_g{}^2$ configuration ($S = 3/2$). The high-spin configuration is in keeping with the optical spectroscopy (see Section 3.6) and reports on similar compounds [53–55]. Vibrational frequency calculations were performed at the same level of theory of the optimized geometries to confirm that there are no imaginary frequencies. The computed vibrational frequencies were achieved using an appropriate scaling factor of 0.967. The electronic spectrum was calculated using time-dependent density functional theory (TD-DFT). Hirshfeld surface analysis in the crystal structure was

Table 2. Selected bond lengths and angles for the title compound.[a,b]

Bond lengths (Å)	Exp.	DFT-calcd.	Bond lengths (Å)	Exp.	DFT-calcd.
Co1–O4	2.010(1)	2.001	Co1–O3	2.061(1)	2.053
Co1–O2	2.104(1)	2.046	Co1–O11^{i}	2.178(1)	1.168
O11–Co1^{i}	2.178(1)	1.175	Co1–N6^{i}	2.107(2)	1.102
Co1–N5	2.082(2)	2.055	N6–Co1^{i}	2.107(2)	1.104
C10–O12	1.230(2)	1.218	C10–O11	1.268(3)	1.262
N5–C9	1.325(3)	1.321	N5–N6	1.377(2)	1.355
N6–C7	1.294(2)	1.293	C7–C10	1.483(3)	1.462
N8–C9	1.357(2)	1.235	C7–N8	1.349(3)	1.342
N21–O23	1.224(3)	1.226	N21–O24	1.236(2)	1.230
C9–N13	1.318(3)	1.315	N21–O22	1.260(3)	1.257
Angles (°)	Exp.	DFT-calcd	Angles (°)	Exp.	DFT-calcd.
O4–Co1–O3	171.8(6)	170.9	O4–Co1–O2	85.8(6)	84.9
O3–Co1–O2	86.4(6)	85.2	O4–Co1–O3	171.8(6)	170.5
O4–Co1–O11^{i}	88.8(5)	88.2	O2–Co1–O11^{i}	89.7(5)	89.6
O3–Co1–O11^{i}	88.7(5)	87.8	O2–Co1–O11^{i}	89.7(5)	89.1
O3–Co1–N5	91.9(6)	91.5	O4–Co1–N5	90.9(6)	90.1
O4–Co1–N6^{i}	96.1(6)	95.5	O3–Co1–N6^{i}	90.9(6)	90.2
O2–Co1–N6^{i}	166.2(5)	165.9	O3–Co1–N5	91.9(6)	90.6
N5–Co1–O2	92.7(6)	91.9	N5–Co1–O11^{i}	177.5(6)	176.9
N5–Co1–O11^{i}	177.5(6)	176.8	N5–Co1–O11^{i}	177.5(6)	175.9
N6^{i}–Co1–O11^{i}	76.7(6)	75.9	N6^{i}–Co1–O11^{i}	76.7(6)	76.2
N5–N6–Co1^{i}	138.6(1)	137.9	N5–Co1–N6^{i}	100.8(6)	100.1
C7–N6–Co1^{i}	113.1(1)	112.5	C10–O11–Co1^{i}	115.4(1)	114.8
C9–N5–Co1	132.9(1)	131.6	N8–C7–C10	128.7(2)	127.9
N6–N5–Co1	120.1(1)	119.8	C7–N8–C9	105.5(2)	105.2
N6–C7–N8	110.7(2)	110.2	C7–N8–H8	127.2(2)	126.5
N6–C7–C10	120.5(2)	119.9	C9–N8–H8	127.2(2)	126.9
N5–C9–N8	109.3(2)	108.7	N13–C9–N5	126.6(2)	126.2
N13–C9–N8	124.1(2)	123.9	C9–N5–N6	106.9(2)	105.8
C7–N6–N5	107.6(2)	107.1	O12–C10–O11	126.8(2)	127.2
O12–C10–C7	119.1(2)	118.6	O11–C10–C7	114.1(2)	113.6
O23–N21–O24	120.7(2)	120.2	O23–N21–O22	119.6(2)	118.9
O24–N21–O22	119.8 (2)	119.2			

[a]Symmetry code: (i) $-x+1, -y+1, -z+1$.
[b]DFT calculations using B3LYP functional and 6-311 + G(2d,2p) basis set for H, C, N, O and LANL2DZ for Co.

performed on the basis of the electron distribution calculated as the sum of spherical atom electron densities [56]. The 3-D Hirshfeld surface mapped with d_{norm} and 2-D fingerprint plots were generated using Crystal-Explorer 3.1 [57]. The fingerprint plots were used to describe various intermolecular interactions including O···H, H···H, N···H, and other contacts present in crystal structure. The crystallographic information file (CIF) was used as input for the analysis.

3. Results and discussion

3.1. Crystal structure

The title compound $[Co_2(Hatzc)_2(H_2O)_6](NO_3)_2{\cdot}4H_2O$ crystallizes in the monoclinic space group $P2_1/n$ with two formula units (Table 1). The unit cell contains two monoanionic Hatzc$^-$ ligands bridging two Co(II) ions in a *N1,N2*-bridging fashion, thus forming a dinuclear complex featuring an almost planar six-membered Co–N–N–Co–N–N– ring (Figure 1). The carboxylic groups of the Hatzc$^-$ ligands form five-membered *N,O*-chelates with the Co(II) centers and three H_2O ligands complete a distorted octahedral coordination. Two nitrate anions and four co-crystallized water molecules complete

Table 3. Selected H bonds for $[Co_2(Hatzc)_2(H_2O)_6](NO_3)_2{\cdot}4H_2O$.

D–H···A	D–H (Å)	H···A (Å)	D···A (Å)	<(DHA)> (°)
O2–H2A···O12^{iii}	0.82	1.92	2.742(2)	177
O2–H2B···O32^{vi}	0.82	1.94	2.740(2)	166
O3–H3A···O23^{vii}	0.82	1.96	2.770(2)	170
O3–H3B···O31	0.82	1.90	2.707(2)	171
O4–H4B···O22^{i}	0.82	1.95	2.756(2)	166
N8–H8···O11^{viii}	0.86	2.02	2.875(2)	163
N13–H13A···O2	0.86	2.12	2.881(2)	147
N13–H13A···O23^{ii}	0.86	2.45	2.987(2)	121
N13–H13B···O12^{iv}	0.86	2.06	2.902(2)	167
O32–H32B···O31^{v}	0.82	2.00	2.805(2)	165
O31–H31A···O22	0.82	1.88	2.697(2)	174
O31–H31B···O11^{iv}	0.82	2.03	2.843(2)	172

Symmetry codes: (i) $1-x, 1-y, 1-z$; (ii) $x, y+1, z$; (iii) $x-1/2, -y+3/2, z+1/2$; (iv) $-x+3/2, y+1/2, -z+1/2$; (v) $-x+1/2, y+1/2, -z+3/2$; (vi) $x-1/2, -y+3/2, z-1/2$; (vii) $-x+1/2, y+1/2, -z+1/2$; (viii) $x-1, y, z$.

the unit cell contents. The Co–O and the Co–N bond lengths are in the range of 2.010(1)–2.178(1) Å and 2.082(2)–2.107(2) Å, respectively (Table 2). They are slightly longer than the corresponding Co–N and Co–O bonds in the recently reported triazole-bridged dinuclear Co(III) complex (μ-5-amino-1,2,4-triazol-1-ide-3-carboxylato-$\kappa^2N^1{:}N^2$)di-μ-hydroxido-$\kappa^4O{:}O$-bis[triamminecobalt(III)] $[Co(NH_3)_3(atzc)(\mu\text{-}OH)_2Co(NH_3)_3]^{2+}$ in the compound $[Co_2(atzc)(OH)_2(NH_3)_6](NO_3)(OH){\cdot}3H_2O$ [38]. In the title compound, an intermetallic Co···Co distance of 4.03(2) Å was found. For the aforementioned dinuclear Co(III) complex $[Co(NH_3)_3(atzc)(\mu\text{-}OH)_2Co(NH_3)_3]^{2+}$, a much shorter Co···Co distance of 2.7918(7) Å was reported which is due to the five-membered Co–N–N–Co–O– ring system in this complex and the very short Co–O_{oxo}–Co unit [38].

In the dinuclear Co(II) complex $[Co_2(Hatzc)_2(H_2O)_6]^{2+}$, the two nitrate anions and the four co-crystallized water molecules are interconnected by a multitude of intramolecular hydrogen bonds (H bonds). The complexes maintain an intramolecular H bond network with two NO_3^- anions (O22) and two water molecules (O31) using their amino function (N13) and one of the water ligands (O2) through N13–H13A···O2, O4–H4B···O22^{i}, O31–H31A···O22, and O3 – H3B···O31 hydrogen bonds (Table 3). These units are interconnected by the nitrates (O23) through intermolecular N13–H13A···O23^{ii} hydrogen bonds, thus forming 1-D undulating chains running parallel to the [100] direction of the unit cell (Figure 2 and Figure S1 in the Supplemental online material). These chains further grow into 2-D layers packed along the *c*-axis of the unit cell through O2–H2A···O12^{iii}, N8–H8···O11^{iv}, N13–H13B···O12^{iv}, and O32–H32B···O31^{v} hydrogen bonds (Figure 2). These layers are finally interconnected to adjacent layers via O2–H2B···O32^{vi}, O3–H3A···O23^{vii}, and O31–H31B···O11^{viii} hydrogen bonds, thus forming a 3-D supramolecular architecture (Figure 2 and Figure S2). Overall, the A···H distances cover a range from 1.88 Å to more than 2.2 Å (Table 3) and are thus assigned to moderate to weak H bonds [58, 59]. Similar extended H bonding networks have been found in other compounds containing the 3-amino-1,2,4-triazole-5-carboxylate ligand [36, 38, 39, 43–46].

3.2. Molecular metrics and DFT-calculated optimized geometry

The optimized geometry of the molecular structure of $[Co_2(Hatzc)_2(H_2O)_6](NO_3)_2{\cdot}4H_2O$ and the metrical data obtained from X-ray diffraction show an excellent agreement (Table 4).

COLOR Online / B&W in Print

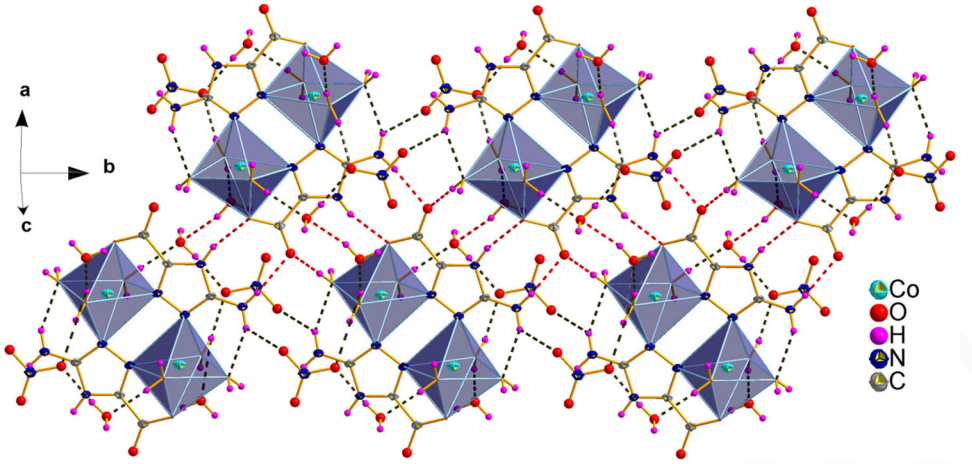


Figure 2. View of the 2-D supramolecular architecture layer of the title compound formed by H bonding interactions represented by dashed red lines.

Table 4. Experimental and DFT-calculated IR and Raman bands with assignments for the title compound.

Exp. IR (cm^{-1})	Calc. IR (cm^{-1})	Exp. Raman (cm^{-1})	Calc. Raman (cm^{-1})	Assignment
3600–3100, broad	3612	3570–3050, broad	–	$\bar{\nu}_{as}$(O–H)
band centered	3580	band centered	–	$\bar{\nu}_{s}$(O–H)
at 3400	3416	at 3400	3460	$\bar{\nu}_{as}(NH_2)$
	3300		3280	$\bar{\nu}_{s}(NH_2)$
	3250		3245	$\bar{\nu}_{as}$(NH)
	3110		3065	$\bar{\nu}_{s}$(NH)
1625	1649	–	1644	$\bar{\nu}$(C = O)
1450	1460	1430	1450	δ(N–H)
–	–	1048	1064	$\bar{\nu}(NO_3^-)$
1040	1070	1030	1020	$\bar{\nu}$(C–C)
820	810	842	835	γ(O–H···O)
750	755	759	745	γ(O–H, ρC–H)
–	–	485	495	δ(C–O)
450	459	461	460	$\omega(NH_2)$
–	–	420	412	τNH_2
–	–	300	295	$\bar{\nu}_{as}$(Co–N)
–	–	265	262	$\bar{\nu}_{s}$(Co–O)
–	–	165	177	γ(N–C–N)

3.3. Hirshfeld surface analysis

The molecular Hirshfeld surface d_{norm} of the unit cell contents was mapped over the d_{norm} range –0.6932 to 1.0254 Å (Figure 3(a)), showing the strongest H bonds as red dots close to the NH_2 group and the H bonding H_2O ligand, fully in line with the crystal structure. Figure 3(b) shows the calculated interstitial voids in the crystal structure of the title compound. These are based on the sum of spherical atomic electron densities at the appropriate nuclear positions (procrystal electron density). The calculation (results under 0.002 a.u. isovalue) shows a volume of the voids of approximately 217 $Å^3$ which makes about 19% of the cell volume and the surface area equal to 493 $Å^2$. However, the voids are very probably not accessible and thus of virtual nature.

The 2-D fingerprint plots (Figure 4) reveal that the O···H/H···O contacts cover 66% of the total surface. The H···H, O···N/N···O, and N···H/H···N contacts comprise 24.7%,

COLOR Online / B&W in Print

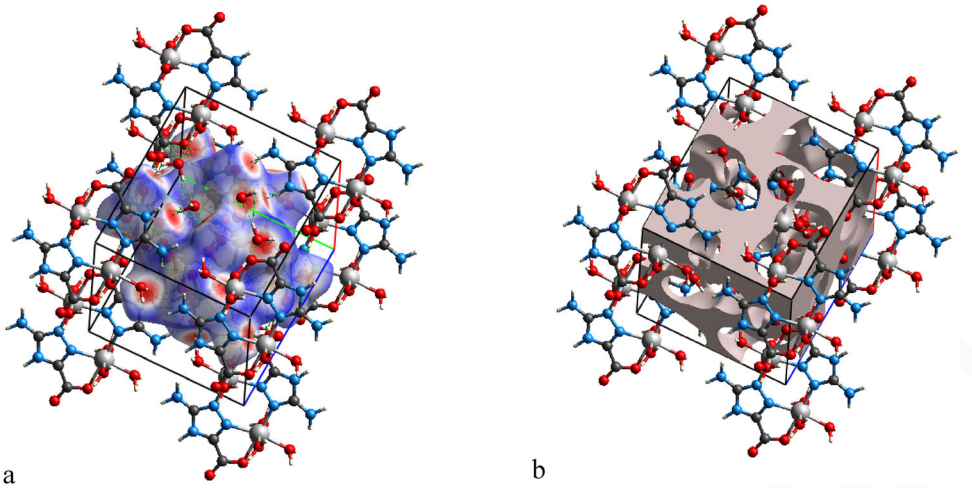


Figure 3. 3-D-Hirshfeld surface of the title compound mapped over d_{norm} (a), and the calculated voids in the crystal structure of the title compound (b).

COLOR Online / B&W in Print

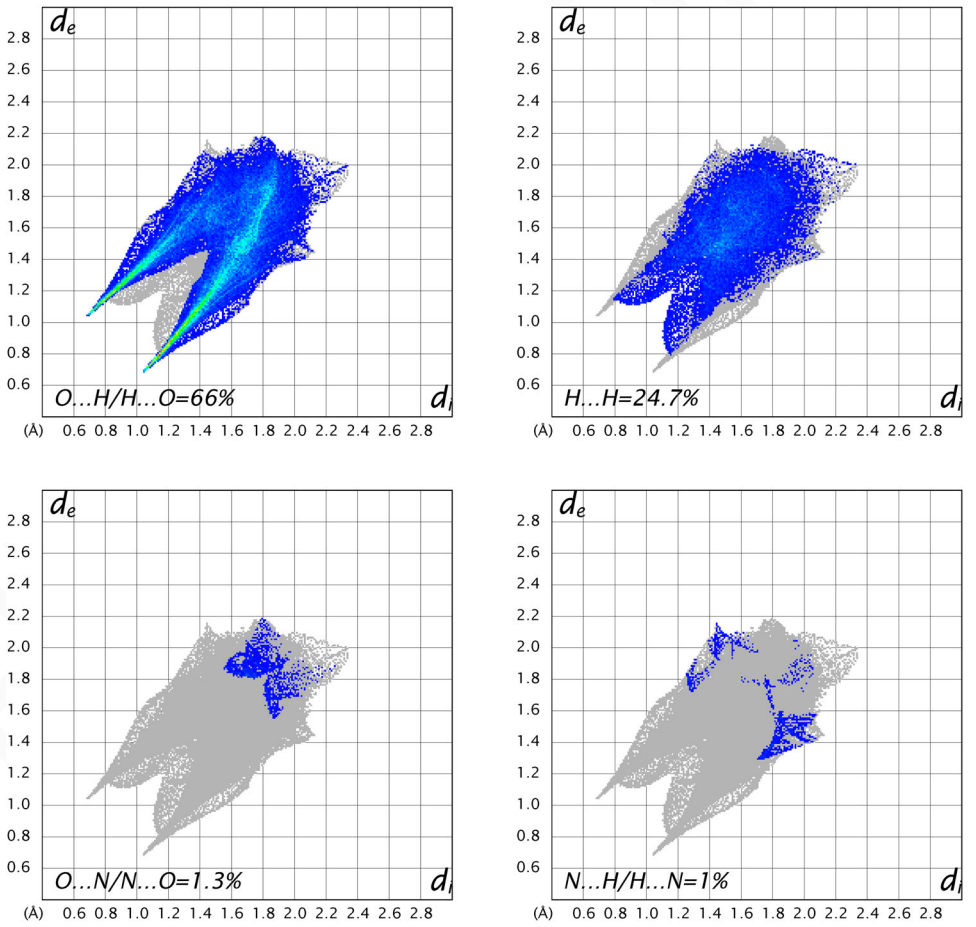


Figure 4. 2-D Fingerprint plots of the title compound.

COLOR Online / B&W in Print

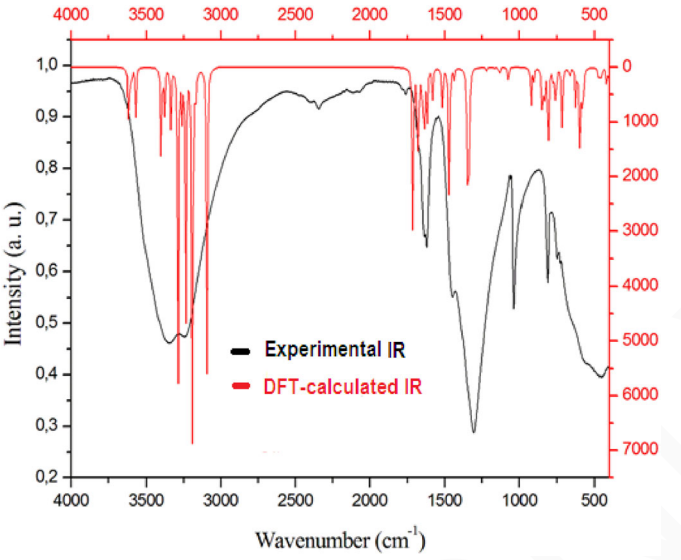


Figure 5. Experimental and DFT-calculated IR spectra of the title compound.

COLOR Online / B&W in Print

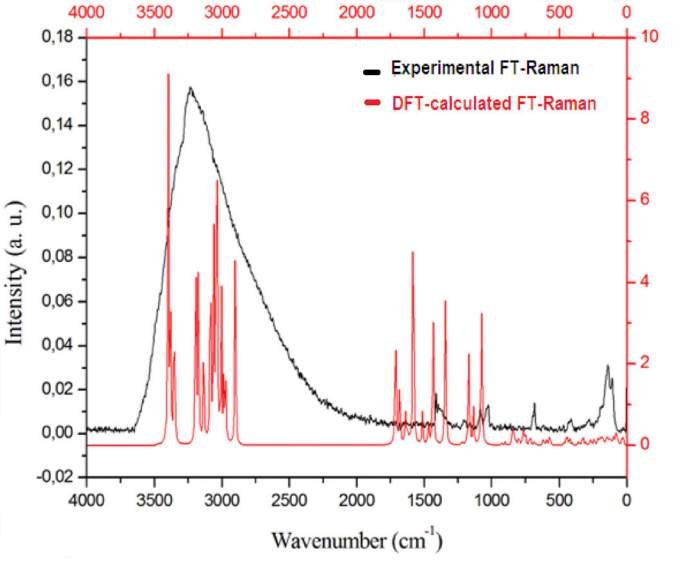


Figure 6. Experimental and DFT-calculated FT-Raman spectra of the title compound.

1.3%, and 1%, respectively, of the total Hirshfeld surface. These results were in good agreement with the structural study, showing that the crystal structure is characterized by a multitude of O–H···O and N–H···O hydrogen bonding interactions.

3.4. Infrared and Raman spectroscopy

The DFT-calculated infrared (IR) (Figure 5) and Raman (Figure 6) spectra agree qualitatively quite well with the experimental data and allow assignments of the most important resonances (Table 4). The broad and intense band at 3400 cm^{-1} in the IR

COLOR Online / B&W in Print

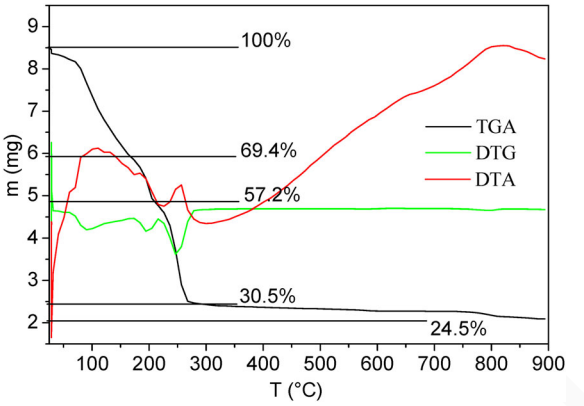


Figure 7. TGA, DTG, and DTA curves of $[Co_2(Hatzc)_2(H_2O)_6](NO_3)_2{\cdot}4H_2O$ (676.19) under argon.

spectrum was assigned to the asymmetric and symmetric O–H, N–H, and NH_2 stretching modes [39, 46, 56, 60]. The broadness of these bands is in line with the presence of both co-crystallized and coordinated water molecules. The assignment of this band is further confirmed by DFT-calculated resonances at 3612, 3580, 3416, 3300, 3250, and 3110 cm^{-1} for the asymmetric and symmetric O–H, NH_2, and N–H stretching vibrations. Bands at 1625 cm^{-1} and 1628 cm^{-1} were assigned to the C = O(R–COO–) stretch of the carboxylic group [22, 46, 55, 61]. The calculation predicts these bands at 1630 and 1640 cm^{-1}. The experimental δ(N–H) band is located at 1450 cm^{-1} [61], whereas the calculations located it at 1460 cm^{-1}. Strong bands at 1040, 820, 750, and 450 cm^{-1} were attributed to $\overline{\nu}$(C–C), γ(O–H···O), γ(O–H, ρC–H), and $\omega(NH_2)$, respectively [62]. The corresponding calculated values of these vibrations appear at 1070, 810, 755, and 459 cm^{-1}, respectively.

Peaks at 1048, 485, and 420 cm^{-1} in the Raman spectrum were attributed to $\overline{\nu}(NO_3^-)$, δ(C – O), and τNH_2, respectively [63, 64]; their corresponding calculated values appear at 1064, 495, and 412 cm^{-1}, respectively. The Co–N and Co–O stretching modes are at 300 and 265 cm^{-1} [55, 64], whereas the calculations predict these bands at 295 and 262 cm^{-1}. In addition, the peak at 165 cm^{-1} was assigned to γ(N–C–N), whereas this peak was calculated at 177 cm^{-1}.

3.5. Thermal analysis

The TGA curve shows that the compound decomposes in three distinct weight loss stages and three endothermic peaks can be found in the DTA (Figure 7). The first mass loss occurred in the range 70–190 °C and can be assigned to loss of the co-crystallized and coordinated water molecules (calculated mass loss: 26.7%; experimental weight loss: 30.6%). A second weight loss was found in the range 190–210 °C and corresponds roughly to the decarboxylation of the compounds (calculated mass loss 13.3%; found 12.2%). Such decarboxylation has been previously reported for compounds of the atzc ligand [40, 65]. The third and final mass loss occurred in the range 210–300 °C leaving a residual mass of about 30%. This step can be assigned to further decomposition of the organic molecules leaving Co(III) oxide Co_2O_3 [66, 67]

COLOR Online / B&W in Print

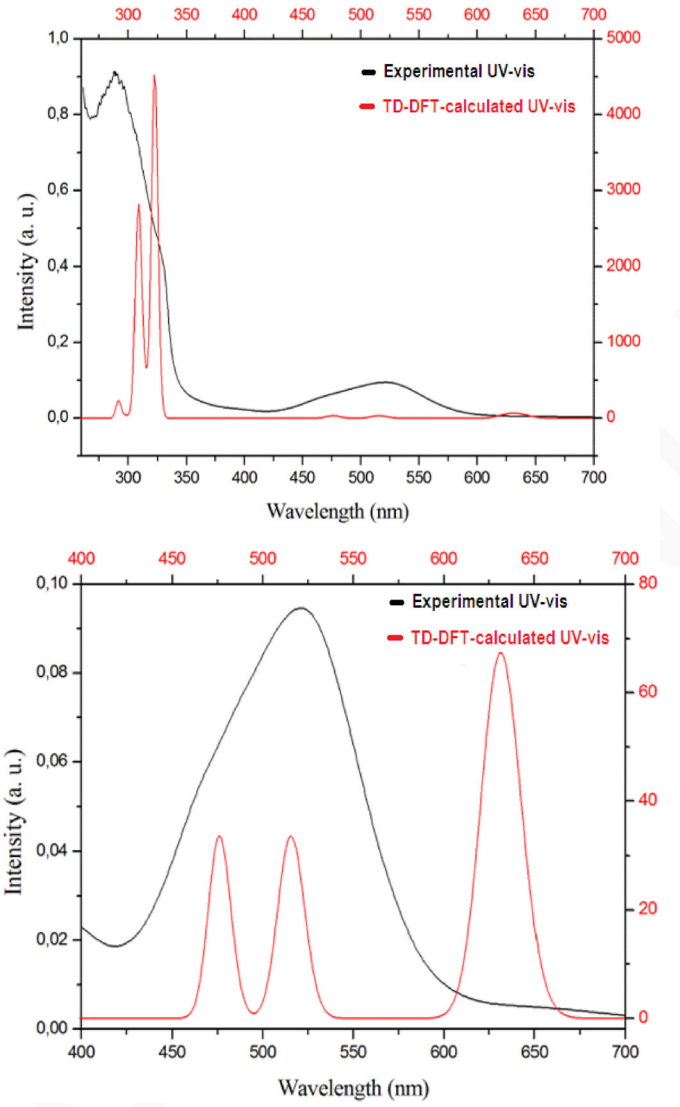


Figure 8. Experimental (in EtOH solution) and TD-DFT-calculated UV–vis absorption spectra of the title compound (top) and zoom in the visible region (bottom).

(calculated: 24.5%). Some residual organic material in this Co_2O_3 is slowly lost upon further heating to 900 °C. This final residue accounts for 24.5 of the original mass and thus precisely the calculated value for Co_2O_3.

3.6. Optical properties

3.6.1. UV–vis absorption spectroscopy

The experimental UV–vis absorption spectrum of the title compound in EtOH solution shows two distinct absorption bands. The intense structured band at 270–340 nm is assigned to π–π* transitions of the ligand, and the broad band peaking at 520 nm is attributed to the d–d transitions in a d^7 high-spin system of Co(II) in an octahedral

COLOR Online / B&W in Print

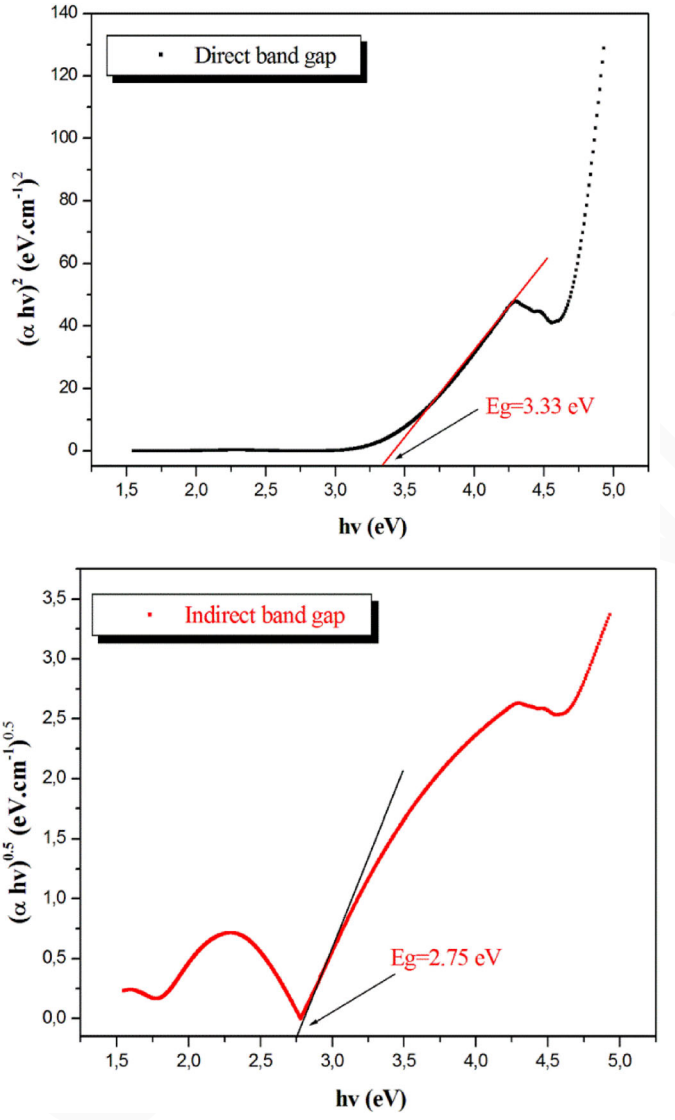


Figure 9. Tauc plots of $(\alpha h\nu)^2$ (top) and $(\alpha h\nu)^{0.5}$ (bottom) versus the photon energy ($h\nu$).

environment (Figure 8) [53, 54, 68]. The TD-DFT calculated spectrum show three transitions in the UV region, confirming the π–π^* assignment (Figure 8, left). The three bands calculated at 475, 519, and 630 nm were attributed to the d–d electronic transitions $^4T_{1g} \rightarrow {}^4T_{2g}$, $^4T_{1g} \rightarrow {}^4A_{2g}$, and $^4T_{1g} \rightarrow {}^4T_{1g}$, respectively (Figure 8, right). These long-wavelength bands agree with the pink color of the material.

For the aqua complex $[Co(H_2O)_6]^{2+}$, the experimental energies for these bands are markedly lower (1250, 625, and 515 nm), while adding Cl^- ligands leads to spectra showing only two bands at 463 and 510 nm, similar to what we observed [68]. The same is true for the UV–vis spectrum of $[Co(NO_3)_2]\cdot 6H_2O$ in molten $[Ca(NO_3)_2]\cdot 4H_2O$, which shows a broad band peaking at 512 nm with a high-energy shoulder at about 480 nm [69, 70]. These two bands were assigned to the $^4T_{1g}(F) \rightarrow {}^4T_{2g}(P)$ and

$^4T_{1g}(F) \rightarrow {}^4A_{2g}(F)$ transitions, respectively [68], thus the observation of the low-energy $^4T_{1g} \rightarrow {}^4T_{2g}$ transition can be hampered for low symmetries, in line with our observation of a weak absorption in this range. The calculated energies fit very well to the experimentally found ones for both the π–π^* and the d–d bands (Figure 8). In contrast to this, the agreement of the calculated relative intensities when comparing the π–π^* and d–d transitions and especially when comparing the three d–d transitions $^4T_{1g} \rightarrow {}^4T_{2g}$, $^4T_{1g} \rightarrow {}^4A_{2g}$, and $^4T_{1g} \rightarrow {}^4T_{1g}$ is poor. Since this mismatch is largest for the highly symmetry-sensitive $^4T_{1g} \rightarrow {}^4T_{1g}$ transition, we assume that tiny deviations of the calculated structure model from the experimental structure are responsible for this.

3.6.2. Optical band gap

The absorption coefficient (α) is a very important parameter for potential optical applications of the compound and was calculated using eq. 1 [71]:

$$\alpha = \frac{2.303 * A}{d} \tag{1}$$

where A is the absorbance and d is the thickness of the path length ($d = 1$ cm).

The optical band gap (E_g) is related to the absorption coefficient (α) and photon energy ($h\nu$) through the Tauc relation (eq. 2) [72]:

$$(\alpha \cdot h\nu) = B(h\nu - E_g)^n \tag{2}$$

where B is a constant, $h\nu$ is the photon energy, and n is the index, which takes different values depending on the mechanism of inter band transitions, with $n = 2$ and $n = 1/2$ corresponding to indirect and direct transitions, respectively [73]. Figure 9(a,b) shows the variations of $(\alpha h\nu)^n$ versus the photon energy ($h\nu$) for different values of n. The E_g value of the title compound was obtained by extrapolating the straight line portion of the curve to $(\alpha \cdot h\nu)^n$ equal to zero. The obtained direct and indirect optical band gap values were 3.33 eV and 2.75 eV, respectively. These band-gap values indicate that the title compound exhibits semiconductor behavior [74].

4. Conclusion

A new compound, $[Co_2(Hatzc)_2(H_2O)_6](NO_3)_2 \cdot 4H_2O$, containing the dinuclear Co(II) complex $[Co_2(Hatzc)_2(H_2O)_6]^{2+}$ was synthesized from 3-amino-1*H*-1,2,4-triazole-5-carboxylic acid (H_2atzc) and $Co(NO_3)_2 \cdot 6H_2O$ by a reflux method. Single-crystal X-ray diffraction revealed that the title compound crystallizes in the centrosymmetric space group $P2_1/n$ of the monoclinic system. The complex network of intra and intermolecular O–H···O and N–H···O hydrogen bonding interactions in the crystal is best described as a succession of mixed layers formed by organic and inorganic ions parallel to the (001) plane stacked along the *c* axis. These layers are further assembled into a 3-D supramolecular architecture through further H bonds. The optimized geometry of the title compound at B3LYP level of theory shows an excellent agreement with the experimental data from the single-crystal X-ray diffraction. The DFT-calculated infrared and Raman spectra are in good agreement with the experimental spectra. Hirshfeld surface analysis confirmed that the structure is dominated by N–H···O and O–H···O interactions. Thermal analysis (TGA and DTA) shows that the title compound is stable

up to 70 °C, a temperature at which the water molecules are released. The UV–vis absorption spectrum is dominated by intense bands at around 280 nm which are assigned to π–π^* transitions, and further contains weaker absorption bands peaking at 520 nm assignable to electronic d–d transitions. TD-DFT calculated excited states agree very well in terms of energy with the experimental data for both π–π^* and the d–d bands. In contrast to this, the match for the relative intensities between calculated π–π^* and d–d transitions and within the set of the three d–d transitions was poor, which might be due to tiny deviations of the calculated geometry from the experimental. The obtained direct and indirect optical band gap values estimated by the Tauc plot method were 3.33 eV and 2.75 eV, respectively. These band-gap values indicate that the title compound exhibits semiconductor behavior. In our future work, we aim to provide more donating groups in the molecular structure to tune the photophysical properties and we will study further properties in view of potential applications of such materials as photodetector.

Disclosure statement

No potential conflict of interest was reported by the author(s).

Funding

SH, YA, and HC thank the Tunisian Ministry of Higher Education and Scientific Research for financial support. This study was also supported by Universität zu Köln. AK acknowledges the University of Cologne for support.

ORCID

Hammouda Chebbi http://orcid.org/0000-0002-0726-7053

References

[1] G. Arroyos, C.M. da Silva, L.B. Theodoroviez, J.E.M. Campanella, R.C.G. Frem. *Chemistry*, **28**, e202103104 (2022).
[2] S. Horike, N. Ma, Z. Fan, S. Kosasang, M.M. Smedskjaer. *Nano Lett.*, **21**, 6382 (2021).
[3] C. Zhang, K. Fan, Y. Chen, Y. Wu, C. Wang. *ACS Appl. Electron. Mater.*, **3**, 1947 (2021).
[4] I. Buta, M.A. Nistor, P. Lönnecke, E. Hey-Hawkins, S.G. Muntean, O. Costisor. *J. Photochem. Photobiol. A*, **404**, 112961 (2021).
[5] L.S. Xie, G. Skorupskii, M. Dincă. *Chem. Rev.*, **120**, 8536 (2020).
[6] L. Feng, K.-Y. Wang, G.S. Day, H.-C. Zhou. *Chem. Soc. Rev.*, **48**, 4823 (2019).
[7] H. Furukawa, K.E. Cordova, M. O'Keeffe, O.M. Yaghi. *Science*, **341**, 1230444 (2013).
[8] T.R. Cook, Y.-R. Zheng, P.J. Stang. *Chem. Rev.*, **113**, 734 (2013).
[9] B. Chen, L. Xu, Z. Xie, W.-Y. Wong. *EcoMat*, **3**, e12106 (2021).
[10] F. Garci, H. Chebbi, A. Klein, M.F. Zid. *J. Coord. Chem.*, **74**, 3182 (2021).
[11] E. San Sebastian, A. Rodríguez-Diéguez, J.M. Seco, J. Cepeda. *Eur. J. Inorg. Chem.*, **2018**, 2155 (2018).
[12] R. Kretschmer. *Chemistry*, **26**, 2099 (2020).
[13] C.E. Housecroft, E.C. Constable. *Chem. Commun. (Camb)*, **56**, 10786 (2020).
[14] B. Ay, N. Doğan, E. Yildiz, İ. Kani. *Polyhedron*, **88**, 176 (2015).

PROOF ONLY

[15] T. Shiga, G.N. Newton, H. Oshio. *Dalton Trans.*, **47**, 7384 (2018).
[16] N.R. Ahmad, A.H. Chughtai, H.A. Younus, F. Verpoort. *Coord. Chem. Rev.*, **280**, 1 (2014).
[17] S. Sun, S. Chen, S. Gao. *J. Coord. Chem.*, **61**, 2068 (2008).
[18] J. Zhou, X.Y. Yun, C. Fang, D.H. Xu, X. Li, Y.Y. Cui, Z.C. Zhang. *Mater. Today Chem.*, **23**, 100757 (2022).
[19] C. Zhou, L.-J. Xu, S. Lee, H. Lin, B. Ma. *Adv. Opt. Mater.*, **9**, 2001766 (2021).
[20] S. Hassen, H. Chebbi, Y. Arfaoui, K. Robeyns, T. Steenhaut, S. Hermans, Y. Filinchuk. *Spectrochim. Acta A Mol. Biomol. Spectrosc.*, **240**, 118612 (2020).
[21] C. Yenikaya, N. Büyükkidan, M. Sari, R. Keşli, H. Ilkimen, M. Bülbül, O. Büyükgüngör. *J. Coord. Chem.*, **64**, 3353 (2011).
[22] Y.-L. Xu, J. Zhang, L.-S. Chen, Y.-Y. Zeng, J.-R. Zhou, C.-L. Ni, W.-X. Zheng. *J. Mol. Struct.*, **1222**, 128902 (2020).
[23] W. Huang, X. Ma, O. Sato, D. Wu. *Chem. Soc. Rev.*, **50**, 6832 (2021).
[24] Y. Yan, A. de Keizer, M.A. Cohen Stuart, N.A.M. Besseling. *Adv. Polym. Sci.*, **242**, 91 (2011).
[25] S. Hassen, H. Chebbi, Y. Arfaoui, M.F. Zid. *J. Iran. Chem. Soc.*, **15**, 2659 (2018).
[26] J. Tong, S. Demeshko, M. John, S. Dechert, F. Meyer. *Inorg. Chem.*, **55**, 4362 (2016).
[27] M.M. Degtyarik, A.S. Lyakhov, L.S. Ivashkevich, V.E. Matulis, V.E. Matulis, S. Gruschinski, S.V. Voitekhovich, B. Kersting, O.A. Ivashkevich. *Dalton Trans.*, **44**, 18518 (2015).
[28] M. Kügler, J. Gałęzowska, F. Schendzielorz, S. Dechert, S. Demeshko, I. Siewert. *Eur. J. Inorg. Chem.*, **2015**, 2695 (2015).
[29] P. Chaudhuri, V. Kataev, B. Büchner, H.-H. Klauss, B. Kersting, F. Meyer. *Coord. Chem. Rev.*, **253**, 2261 (2009).
[30] G.B. Deacon, R.J. Phillips. *Coord. Chem. Rev.*, **33**, 227 (1980).
[31] P. Teo, T.S.A. Hor. *Coord. Chem. Rev.*, **255**, 273 (2011).
[32] X. Zhang, N. Xing, F. Bai, L. Wan, H. Shan, Y. Hou, Y.-H. Xing, Z. Shi. *CrystEngComm*, **15**, 9135 (2013).
[33] H. Benaissa, M. Wolff, K. Robeyns, G. Knör, K. Van Hecke, N. Campagnol, J. Fransaer, Y. Garcia. *Cryst. Growth Des.*, **19**, 5292 (2019).
[34] Y.P. Petrenko, D.M. Khomenko, R.O. Doroshchuk, S. Shova, G. Novitchi, K. Piasta, E.G. Kontecka, R.D. Lampeka. *Inorg. Chim. Acta*, **500**, 119216 (2020).
[35] Y. Li, Z.-X. Wang, C.-G. Zhang, Q. Liu, L. Liu. *Inorg. Chem. Commun.*, **38**, 58 (2013).
[36] B. Li, H. Song, H. Wu, J. Wang, X. Tian, X. Ma. *J. Coord. Chem.*, **74**, 1159 (2021).
[37] K. Wang, Z. Wang, J. Liu, C. Li, F. Mao, H. Wu, Q. Zhang. *ACS Appl. Mater. Interfaces*, **12**, 47482 (2020).
[38] F.Y. Liu, D.M. Zhou, X.L. Zhao, J.F. Kou. *Acta Crystallogr. C Struct. Chem.*, **73**, 1010 (2017).
[39] B. Liu, J.A. Fernandes, J.P.C. Tomé, F.A. Almeida Paz, L. Cunha-Silva. *Molecules*, **20**, 12341 (2015).
[40] J.-J. Hou, X. Xu, N. Jiang, Y.-Q. Wu, X.-M. Zhang. *J. Solid State Chem.*, **223**, 73 (2015).
[41] J. Hernández-Gil, S. Ferrer, A. Castiñeiras, F. Lloret. *Inorg. Chem.*, **51**, 9809(2012).
[42] K.S. Asha, A.C. Reber, A.F. Pedicini, S.N. Khanna, S. Mandal. *Eur. J. Inorg. Chem.*, **2015**, 2085 (2015).
[43] R. Bouchene, S. Bouacida, F. Berrah, T. Roisnel. *Acta Crystallogr. C Struct. Chem.*, **70**, 672 (2014).
[44] J.A. Fernandes, B. Liu, J.P.C. Tome, L. Cunha-Silva, F.A. Almeida Paz. *Acta Crystallogr. E Struct. Rep. Online*, **67**, o2073 (2011).
[45] Y.F. Wang, X.Y. Sun, J.L. Geng. *Russ. J. Coord. Chem.*, **42**, 143 (2016).
[46] J.-Y. Gao, N. Wang, X.-H. Xiong, C.-J. Chen, W.-P. Xie, X.-R. Ran, Y. Long, S.-T. Yue, Y.-L. Liu. *CrystEngComm*, **15**, 3261 (2013).
[47] G.M. Sheldrick. *Acta Crystallogr. A Found. Adv.*, **71**, 3 (2015).
[48] G.M. Sheldrick. *SHELXL-2014 Program for the Refinement of Crystal Structures*, University of Göttingen, Göttingen, Germany (2014).
[49] M.J. Frisch, G.W. Trucks, H.B. Schlegel, G.E. Scuseria, M.A. Robb, J.R. Cheeseman, G. Scalmani, V. Barone, B. Mennucci, G.A. Petersson, H. Nakatsuji, M. Caricato, X. Li, H.P. Hratchian, A.F. Izmaylov, J. Bloino, G. Zheng, J.L. Sonnenberg, M. Hada, M. Ehara, K.

Toyota, R. Fukuda, J. Hasegawa, M. Ishida, T. Nakajima, Y. Honda, O. Kitao, H. Nakai, T. Vreven, J.A. Montgomery, Jr., J.E. Peralta, F. Ogliaro, M. Bearpark, J.J. Heyd, E. Brothers, K.N. Kudin, V.N. Staroverov, R. Kobayashi, J. Normand, K. Raghavachari, A. Rendell, J.C. Burant, S.S. Iyengar, J. Tomasi, M. Cossi, N. Rega, J.M. Millam, M. Klene, J.E. Knox, J.B. Cross, V. Bakken, Adamo, J. Jaramillo, R. Gomperts, R.E. Stratmann, O. Yazyev, A.J. Austin, R. Cammi, C. Pomelli, J.W. Ochterski, R.L. Martin, K. Morokuma, V.G. Zakrzewski, G.A. Voth, P. Salvador, J.J. Dannenberg, S. Dapprich, A.D. Daniels, O. Farkas, J.B. Foresman, J.V. Ortiz, J. Cioslowski, J. Fox. *Gaussian 09, Revision A.1*, Gaussian, Inc., Wallingford, CT (2009).

[50] R.G. Parr, W. Yang. *Density Functional Theory of Atoms and Molecules*, Oxford University Press, Oxford (1989).

[51] R. Krishnan, J.S. Binkley, R. Seeger, J.A. Pople. *J. Chem. Phys.*, **72**, 650 (1980).

[52] S. Hassen, H. Chebbi, M.F. Zid, Y. Arfaoui. *J. Mol. Struct.*, **1167**, 1 (2018).

[53] I. Krivokapic, M. Zerara, M.L. Daku, A. Vargas, C. Enachescu, C. Ambrus, P. Tregenna-Piggott, N. Amstutz, E. Krausz, A. Hauser. *Coord. Chem. Rev.*, **251**, 364 (2007).

[54] M.H. Sadhu, S.B. Kumar, J.K. Saini, S.S. Purani, T.R. Khanna. *Inorg. Chim. Acta*, **466**, 219 (2017).

[55] J. Sun, K.-X. Shang, Y.-J. Wu, Q. Zhang, X.-Q. Yao, Y.-X. Yang, D.-C. Hu, J.-C. Liu. *Polyhedron*, **141**, 223 (2018).

[56] M.A. Spackman, P.G. Byrom. *Chem. Phys. Lett.*, **267**, 215 (1997).

[57] S.K. Wolff, D.J. Greenwood, J.J. McKinnon, D. Jayatilaka, M.A. Spackman. *Crystal Explorer*, (2012).

Q2

[58] R.S. Rathore, Y. Alekhya, A.K. Kondapi, K. Sathiyanarayanan. *CrystEngComm*, **13**, 5234 (2011).

[59] T. Steiner. *Angew. Chem. Int. Ed.*, **41**, 48 (2002).

[60] M. Mondelli, F. Pavan, P.C. de Souza, C.Q. Leite, J. Ellena, O.R. Nascimento, G. Facchin, M.H. Torre. *J. Mol. Struct.*, **1036**, 180 (2013).

[61] X.-Y. Zhang, Z.-Y. Liu, Y.-F. Xia, Y.-Y. Zhang, E.-C. Yang, X.-J. Zhao. *J. Coord. Chem.*, **66**, 4399 (2013).

[62] N. Ennaceur, R. Henchiri, B. Jalel, M. Cordier, I. Ledoux-Rak, E. Elaloui. *J. Mol. Struct.*, **1144**, 25 (2017).

[63] M.A. Kandhaswamy, V. Srinivasan. *Bull. Mater. Sci.*, **25**, 41 (2002).

[64] A. Wesełucha-Birczyńska, C. Paluszkiewicz. *J. Mol. Struct.*, **614**, 339 (2002).

[65] B. Liu, H.-J. Feng, Z.-H. Zhang, L. Xu, H. Jiao. *J. Mol. Struct.*, **1098**, 240 (2015).

[66] M.L. Dianu, A. Kriza, A.M. Musuc. *J. Therm. Anal. Calorim.*, **112**, 585 (2013).

[67] M.S. Masoud, E.A. Khalil, A.M. Ramadan. *J. Anal. Appl. Pyrolysis*, **78**, 14 (2007).

[68] M. Uchikochi. *J. Sol. Chem.*, **47**, 2021 (2018).

[69] I.J. Zsigrai, S.B. Gadzuric, R. Nikolic, L. Nagy. *Z. Naturforsch. A*, **59**, 604 (2004).

[70] M. Vranes, S.B. Gadzuric, I.S. Zsigrai, D. Dozic. *J. Mol. Liq.*, **152**, 34 (2010).

[71] A. Eshaghi, A. Graeli. *Optik Int. J. Light Electron. Opt.*, **125**, 1478 (2014).

[72] A. Ayeshamariam, S. Ramalingam, M. Bououdina, M. Jayachandran. *Spectrochim. Acta A Mol. Biomol. Spectrosc.*, **118**, 1135 (2014).

[73] P. Makuła, M. Pacia, W. Macyk. *J. Phys. Chem. Lett.*, **9**, 6814 (2018).

Q3 [74] E. Rosencher, B. Vinter. *Optoelectronics*, Cambridge University Press (2002).

Proof Only